The proliferation of human mucosal-associated invariant T cells requires a MYC-SLC7A5-glycolysis metabolic axis

Kedia-Mehta, Nidhi; Pisarska, Marta M; Rollings, Christina; O'Neill, Chloe; De Barra, Conor; Foley, Cathriona; Wood, Nicole A W; Wrigley-Kelly, Neil; Veerapen, Natacha; Besra, Gurdyal; Bergin, Ronan; Jones, Nicholas; O'Shea, Donal; Sinclair, Linda V; Hogan, Andrew E

DOI:
10.1126/scisignal.abo2709

Document Version
Peer reviewed version

Citation for published version (Harvard):
Kedia-Mehta, N, Pisarska, MM, Rollings, C, O'Neill, C, De Barra, C, Foley, C, Wood, NAW, Wrigley-Kelly, N, Veerapen, N, Besra, G, Bergin, R, Jones, N, O'Shea, D, Sinclair, LV & Hogan, AE 2023, 'The proliferation of human mucosal-associated invariant T cells requires a MYC-SLC7A5-glycolysis metabolic axis', *Science signaling*, vol. 16, no. 781, eabo2709. https://doi.org/10.1126/scisignal.abo2709

Editor's summary:

The master regulator of innate T cell metabolism

Mucosal associated invariant T (MAIT) cells are a type of innate-like T cells that are enriched in adipose, gut, and liver tissue and that recognize bacterial metabolites. Upon activation, they proliferate and produce cytokines to promote host defense. Kedia-Mehta et al. showed that MAIT proliferation depended on MYC-associated pathways involving amino acid transport and glycolysis. Furthermore, MAIT cells from patients with obesity showed disrupted function and engagement of these pathways. These findings demonstrate that the canonical metabolic pathways found in conventional T cells are active in MAIT cells and may be relevant to the development of MAIT cell-based therapies and the study of obesity. -AEB

The proliferation of human mucosal associated invariant T cells requires a MYC-SLC7A5-glycolysis metabolic axis

Nidhi Kedia-Mehta[1*], Marta M. Pisarska[1,2*], Christina Rollings[3], Chloe O'Neill[2], Conor De Barra[2], Cathriona Foley[4], Nicole AW. Wood[1,2], Neil Wrigley-Kelly[5], Natacha Veerapen[6], Gurdyal Besra[6], Ronan Bergin[2], Nicholas Jones[7], Donal O'Shea[2,5], Linda V. Sinclair[3#] and Andrew E. Hogan[1,2#]

Affiliations: [1.]Kathleen Lonsdale Institute for Human Health Research, Maynooth University, Maynooth, Co Kildare. Ireland. [2.]National Children's Research Centre, Dublin 12, Ireland. [3.] Division of Cell Signaling and Immunology, School of Life Sciences, University of Dundee, United Kingdom. [4.]Department of Biological Sciences, Munster Technological University, Cork, Ireland. [5.] St Vincent's University Hospital & University College Dublin, Dublin 4, Ireland. [6.] School of Biosciences, University of Birmingham, United Kingdom. 7. Institute of Life Science, Swansea University Medical School, Swansea, United Kingdom.

*These authors contributed equally to this study.
[#]Joint Senior Authors.

Address for correspondence:
Dr Andrew E. Hogan –
Email: Andrew.E.Hogan@mu.ie

Dr Linda V. Sinclair -
Email: L.V.Sinclair@dundee.ac.uk

Running title: MYC controls MAIT cell proliferation

Keywords: Mucosal associated invariant T cells, Metabolism, MYC, Proliferation, Obesity

Abstract

Mucosal associated invariant T (MAIT) cells are an abundant population of innate T cells that recognize bacterial ligands and play a key role in host protection against bacterial and viral pathogens. Upon activation, MAIT cells undergo proliferative expansion and increase their production of effector molecules such as cytokines. In this study, we found that mRNA and protein the abundance of the key metabolism regulator and transcription factor MYC was increased in stimulated MAIT cells. Using quantitative mass spectrometry, we identified the activation of two MYC controlled metabolic pathways, amino acid transport and glycolysis, both of which were necessary for MAIT cell proliferation. Finally, we showed that MAIT cells isolated from people with obesity showed decreased *MYC* mRNA abundance upon activation, which was associated with defective MAIT cell proliferation and functional responses. Collectively, our data uncovers the importance of MYC-regulated metabolism for MAIT cell proliferation and provides additional insight into the molecular basis for the functional defects of MAIT cells in obesity.

64 **Introduction**

65 Mucosal Associated Invariant T (MAIT) cells are a population of non-MHC restricted T
66 cells that are important in the immune defence against bacterial and viral infections[1,
67 2, 3, 4, 5]. In addition to their abundance (2-10% of total T cells) in peripheral blood, MAIT
68 cells are relatively abundant across of range of human tissues including adipose, gut
69 and the liver where they can account for up to 50% of all T cells[6]. MAIT cells are early
70 responding T cells that are capable of producing multiple cytokines rapidly upon
71 activation such as IFN-γ, TNF and IL-17[1, 7]. Due to their robust production of effector
72 molecules, MAIT cells have been implicated in both host protection (against
73 pathogens[6] and cancer cells[8]) and tissue repair[9, 10, 11]. MAIT cells are activated when
74 their invariant T cell receptor (TCR) recognise bacterial derivatives presented on the
75 MHC-like molecule MR1[5, 7]. MAIT cells can also be activated in a T cell receptor-
76 independent manner, through cytokine stimulation[10, 12]. Altered MAIT cell cytokine
77 profiles have been reported in several diseases including obesity, arthritis, and viral
78 infection[13, 14, 15, 16, 17, 18].

79

80 One key functional response of MAIT cells is their ability to proliferate rapidly upon
81 activation, which has been demonstrated both in vitro and in vivo[19, 20, 21]. Increased
82 immune signal-driven proliferation relies upon metabolic reprogramming to provide
83 the large amounts of energy and biosynthetic intermediates needed to support the
84 rapid generation of new cells[22]. In conventional T cells, metabolic reprogramming in
85 response to activation is controlled by the transcription factor MYC, which acts as a
86 master metabolic regulator[23]. MYC expression is rapidly induced after T cell receptor
87 (TCR) stimulation, and is sustained by amino acid availability and Interleukin 2 (IL-2)
88 signalling[24, 25,26]. In particular, the expression of the amino acid transporter SLC7A5,
89 which is under the control of MYC, forms a forward feeding loop in which amino acid
90 transport through SLC7A5 sustains MYC protein expression[24]. Whether MYC acts as a
91 metabolic regulator in MAIT cells is currently unknown. Although it is known that MAIT
92 cell cytokine production is dependent on glycolytic metabolism, it is unclear what
93 regulates and fuels MAIT cell proliferation[27]. To address these unknowns, we have
94 interrogated the molecular and metabolic requirements for MAIT cell proliferation. In
95 addition, defective Natural Killer (NK) and MAIT cell metabolism and defective cellular

96 responses are present in people with obesity, which may translate to elevated
97 incidences of co-morbid diseases[27, 28, 29]. However, the impact of obesity on important
98 metabolic regulators such as MYC are not clearly understood and remain to be
99 elucidated.
100
101 Using quantitative mass spectrometry, we identified a robust upregulation of MYC
102 expression and MYC controlled metabolic pathways in stimulated MAIT cells. We
103 showed that MYC-regulated metabolic pathways (including amino acid transport and
104 glycolysis) are essential for human MAIT cell proliferation. Finally, we showed that
105 obesity is associated with defective MAIT cell proliferation, due to a defective MYC-
106 SLC7A5-Glycolysis metabolic axis. Collectively, our data demonstrated that MYC acts
107 as a metabolic regulator in TCR and cytokine stimulated MAIT cells and that this is
108 essential for proliferation, and provides further molecular insight into obesity related
109 defects in human MAIT cells.
110
111 **RESULTS**
112 **MAIT cells remodel their proteomes upon TCR activation.**
113 To investigate the major pathways regulating MAIT cell activation, we performed
114 quantitative mass spectrometry on MAIT cells expanded by treatment with IL-2
115 ($MAIT^{IL-2}$ cells) before and after TCR stimulation (anti-TCR/CD28 and IL-12/IL-18;
116 $MAIT^{STIM}$). We identified 5740 proteins in both IL-2 maintained and stimulated MAIT
117 cells and have estimated the absolute protein copy number per cell using the
118 proteomic ruler method which uses the mass spectrometry signal of histones as an
119 internal standard[30] (Supplementary File 1). Only a small proportion of highly abundant
120 proteins account for the majority of cellular mass in conventional effector T cells[24, 31,
121 32]; in human MAIT cells, we found that expression of 8 proteins (Supplementary Figure
122 1) contribute 25% of the total mass, and expression abundance of approximately 350
123 proteins accounts for 75 % of the total cellular mass (Figure 1A) Upon TCR activation,
124 we observed remodelling of the $MAIT^{IL-2}$ cell proteome (Figure 1B), which was
125 accompanied by an increase in total protein mass and cell size (Figure 1C-D). The
126 expression of the most abundant proteins did not change after stimulation and
127 remained proportional to the amounts expressed basally in $MAIT^{IL-2}$ cells

128 (Supplementary Figure 1). Signature effector proteins such as Interferon gamma
129 (IFNG) and Granzyme B (GRZB) were amongst the most highly increased proteins upon
130 stimulation (Figure 1E-F). We were also able to detect many proteins associated with
131 a core MAIT cell signature; including IL-18R1 (which strongly increased expression in
132 response to stimulation), KLRB1 (moderate increase), DPPIV (moderately decreased),
133 and TRAV1-2 (expression is decreased upon stimulation) (Figure 1E). In total, 780
134 proteins were increased more than 1.5-fold upon activation (Figure 1B&F). Pathway
135 analysis highlighted that the increased proteins were enriched in multiple processes
136 and included a large proportion involved in governing cellular metabolism (Figure 1G).
137

138 **MAIT cells upregulate expression of the transcription factor MYC and its**
139 **downstream target pathways upon activation.**

140 In silico pathway analysis of a previously published RNA sequencing data-set [10]
141 revealed that MAIT cells activated ex vivo ($MAIT^{EX\text{-}VIVO}$ cells) have a strong MYC
142 signature as determined by the Hallmark gene set enrichment analysis (Figure 2A &
143 Supplementary Figure 2). In our activated human $MAIT^{IL\text{-}2}$ proteomic dataset, we also
144 found increased MYC expression and its target proteins (Figure 2B-C). Using
145 alternative methods to measure MYC expression, we show MYC protein expression is
146 increased in $MAIT^{IL2}$ stimulated through their TCR (Figure 2D-E). We next interrogated
147 MYC expression in TCR stimulated $MAIT^{EXVIVO}$ cells (Figure 2F-G). Together these data
148 show MYC is increased in response to TCR stimulation in both $MAIT^{EX\ VIVO}$ and $MAIT^{IL2}$
149 expanded cells. To further support the increased expression of MYC targets in
150 activated MAIT cells, we analyzed another published RNA sequencing data set[11], and
151 once again saw increased MYC target gene expression in activated MAIT cells (Figure
152 2H & Supplementary Figure 3). TCR activation induces MYC expression in conventional
153 $CD8^+$ T cells[26] . Furthermore, MYC expression is maintained by IL-2 through the
154 activation of JAK/STAT signaling pathways[26]. With this in mind we interrogated the
155 upstream signals required for MYC activation in MAIT cells. We compared the ability
156 of TCR stimulation and the cytokines IL-2, IL-12 and IL-18 to induce MYC expression in
157 $MAIT^{IL\text{-}2}$ cells, with TCR triggering induced the strongest MYC expression
158 (Supplementary Figure 4).
159

160 [26]. Analysis of the MAIT^{IL-2} proteomic data showed that upon activation, MAIT cells
161 had increased abundance of STAT5 but not STAT3 (Figure 2I-K). Furthermore,
162 inhibition of STAT5 activation reduced MYC expression in TCR-activated MAIT cells
163 (Figure L-M).
164
165 **MAIT cell proliferation is dependent on MYC**
166 MAIT cells can readily proliferate upon TCR activation with a cognate antigen or
167 bacterial infection[20, 21]. To build on these observations, we investigated the ability of
168 MAIT$^{EX-VIVO}$ cells to proliferate in vitro after stimulation with the riboflavin metabolite
169 5-ARU, which is further processed into the MAIT cell cognate antigen 5-OP-RU,
170 resulting in a full antigenic stimulation through the TCR. MAIT$^{EX-VIVO}$ cells activated
171 with antigenic stimulation failed to proliferate despite increased expression of
172 activation markers such the interleukin 2 receptor alpha chain, CD25 (Figure 3A-C).
173 Increased expression of CD25 was also noted on MAIT^{IL-2} cells after TCR bead
174 stimulation (Figure 3D). IL-2 is a driver of T cell growth and proliferation[33], so we
175 investigated whether the addition of IL-2 alongside antigenic stimulation could drive
176 MAIT$^{EX-VIVO}$ cell proliferation. Addition of IL-2 resulted in significant MAIT cell growth
177 and proliferation in combination with antigenic stimulation (Figure 3E-G). MYC
178 expression is required for conventional T cell blasting and proliferation in response to
179 TCR signalling[23, 24]. Many of the transcriptional programs driven by MYC are
180 dependent upon dimerization with MAX[34]. The MYC inhibitor 10074-G5 blocks the
181 binding of MAX to MYC and thereby inhibits transcriptional activity[35]. Using this
182 inhibitor, we saw that the increase in cell size and CD25 expression in MAIT cells after
183 TCR simulation was dependent on MYC activity (Figure 3H-I). Furthermore, MYC
184 activity was required for MAIT cell proliferation in response to TCR and IL-2 (Figure 3J
185 & Supplementary Figure 5).
186
187 **The MYC-controlled amino acid transporter SLC7A5 is required for MAIT cell**
188 **proliferation.**
189 Proliferation is a metabolically intense process, requiring large amounts of energy and
190 de novo generation of biosynthetic intermediates, so we next investigated metabolic
191 processes under the control of MYC. In conventional murine T cells, TCR-driven

192 expression of MYC induces the expression of critically important amino acid
193 transporters, including SLC7A5[24]. SLC7A5 and its heavy chain chaperone, CD98
194 (SLC3A2), form the heterodimeric large neutral amino acid transporter (LAT-1).
195 Interrogation of the MAIT cell proteomes show that *SLC7A5* expression increases from
196 25000 copies per cell in $MAIT^{IL-2}$ cells to 50000 copies per cell in $MAIT^{IL-2+STIM}$ cells
197 (Figure 4A) which correlates with increased mRNA expression in $MAIT^{IL-2+STIM}$
198 compared with $MAIT^{IL-2}$ cells (Figure 4B). We also noted increased expression of the
199 CD98/SLC3A2 (Figure 4C-D). Together these data show that that upon TCR activation
200 both $MAIT^{EX-VIVO}$ and $MAIT^{IL-2}$ cells increase the expression of SLC7A5 protein, *SLC7A5*
201 mRNA and CD98 surface expression (Figure 4A-C). Using a flow cytometry-based
202 assay, uptake of kynurenine, a fluorescent SLC7A5 substrate, was monitored in MAIT
203 cells. $MAIT^{EX-VIVO}$ cells exhibited low kynurenine uptake, however upon TCR/cytokine
204 stimulation, $MAIT^{EX-VIVO}$ cells rapidly increase transport through SLC7A5 (Figure 4E).
205 From our proteomic analysis we also noted that upon activation MAIT cells increase
206 expression of several other amino acid transporters, including SLC1A5, SLC7A1, and
207 SLC38A1, which are also controlled by MYC[24] (Supplementary Figure 6). We used MYC
208 inhibitors to investigate whether the TCR/cytokine driven increase in LAT-1 expression
209 was dependent upon MYC activity. Inhibition of MYC resulted in reduced *SLC7A5*
210 mRNA expression as well as reduced CD98 expression in activated MAIT cells (Figure
211 4F-G). Furthermore, inhibition of MYC reduced the uptake of the SLC7A5 substrate
212 kynurenine by activated MAIT cells (Figure 4H). Next, we investigated if loss of amino
213 acid transport via LAT-1 impacted MAIT cell proliferation. Using the competitive
214 substrate BCH to block LAT-1 activity, we showed that MAIT cell proliferation is limited
215 when uptake through LAT-1 is blocked. Therefore, SLC7A5 activity during TCR/IL-2
216 activation is required for $MAIT^{EX-VIVO}$ cell proliferation (Figure 4I-K).
217
218 **Glucose metabolism supports MAIT cell proliferation.**
219 MYC has been highlighted as a master regulator of glycolysis[23, 24], and therefore we
220 investigated whether glucose metabolism was required for MAIT cell proliferation. We
221 have reported that MAIT cells had increased glycolytic metabolism upon activation[27],
222 here, we noted increased expression of the glycolytic enzymes (hexokinase-II (HKII)
223 and lactate dehydrogenase (LDH)) in both $MAIT^{EX-VIVO}$ and $MAIT^{IL-2}$ cells following TCR

224 stimulation (Figure 5A-D). Inhibition of MYC resulted in diminished *HKII* mRNA
225 expression in activated MAIT$^{EX\text{-}VIVO}$ cells (Figure 5E). We also showed that inhibition of
226 MYC limited the rates of glycolytic metabolism in TCR activated MAIT cells (Figure 5F-
227 G). To investigate whether glucose metabolism is required for MAIT cell proliferation,
228 we treated MAIT cells with the glycolytic inhibitor 2-deoxy-D-glucose (2DG). MAIT cell
229 proliferation was inhibited when treated with 2DG (Figure 5H-J). Limiting the glucose
230 availability in the culture media from 10mM to 1mM reduced MAIT cell proliferation
231 (Figure 5K-L). Finally, replacing the carbon source in the culture media from glucose
232 to galactose (which slows the rates of glycolysis[36]) resulted in reduced MAIT cell
233 proliferation (Figure 5M).
234
235 **MAIT cells from people with obesity display blunted MYC expression and fail to**
236 **proliferate.**
237 MAIT cell frequencies and cytokine production are altered in people with obesity
238 (PWO)[14, 37, 38]. We investigated the proliferative capacity of MAIT cells from PWO in
239 response to a combination of antigenic (5-ARU-MG) and cytokine (IL-2) stimulation.
240 MAIT cells from PWO displayed defective proliferation in response to immune
241 stimulation when compared to healthy controls (Figure 6A-B, Supplementary Figure
242 7) . These data provided further evidence that MAIT cells are functionally impacted by
243 obesity. Having highlighted the critical importance of MYC for MAIT cell proliferative
244 responses, we assessed MYC expression in cohorts of PWO and healthy controls, and
245 found impaired induction of MYC expression in MAIT$^{EX\text{-}VIVO}$ cells in response to
246 immune activation from PWO (Figure 6C-D). Targeted analysis of a previously
247 published RNA sequencing data set on MAIT cells isolated from PWO and healthy
248 controls[27], showed reduced expression of MYC target gene expression in MAIT cells
249 from PWO (Figure 6E). *MYC* RNA expression in these same individuals was not reduced
250 (Figure 6F), indicating that signalling downstream of immune activation to drive
251 expression of MYC RNA was not impaired. Since CD25 surface protein expression was
252 reduced with MYC inhibition (Figure 3H), we measured CD25 expression on MAIT cells
253 from PWO, and found diminished CD25 levels in response to TCR and cytokine
254 activation (Figure 6G). Having identified that SLC7A5, a direct transcriptional target of
255 MYC, is critical for MAIT cell proliferation in response to immune stimulation, we

256 measured SLC7A5 expression on MAIT cells from PWO. We demonstrated that upon
257 activation MAIT cells from PWO express significantly less *SLC7A5* mRNA and CD98,
258 resulting in reduced amino acid transport, a process necessary for proliferation (Figure
259 6H-J).
260
261 **Discussion**
262 MAIT cells are a subset of unconventional T cells which are abundant in human blood
263 and tissues, including liver and adipose tissue[6, 39]. MAIT cells are capable of responding
264 rapidly to stimulation by producing cytokines and lytic molecules, and proliferating[6].
265 Due to their potent effector functions and abundance, MAIT cells have been shown to
266 play an important role in the host defence against pathogens and malignancies[1, 8], and
267 are of interest as a potential immunotherapeutic agent[21, 40]. However, the molecular
268 regulation of MAIT cell effector functions are still emerging. In the current study, we
269 demonstrated that MAIT cell proliferation is dependent on the transcription factor
270 MYC. We showed that upon activation, MAIT cells had a greater abundance of MYC
271 target proteins, including SLC7A5 and HKII, which are both integral to key processes
272 required for MAIT cell proliferation. Finally, we showed that MYC expression and
273 targets under the controls of MYC are defective in people with obesity, underpinning
274 diminished MAIT cell proliferation (Figure 7). These observations suggest a
275 mechanism which may increase host susceptibility to infection and malignancies.
276
277 Quantitative mass spectrometry allows a high-dimensional analysis of the proteome
278 and activation induced remodelling[24, 25, 26]. Using this approach, we were able to
279 identify 5740 proteins in both resting IL-2 expanded MAIT cells and stimulated IL-2
280 expanded MAIT cells, similar to previously published data sets[41, 42]. TCR and cytokine
281 stimulation were associated with the remodelling of the MAIT cell proteome and were
282 associated with significant increases in protein content and cell size. Pathway analysis
283 of our proteomic dataset and previously published RNA sequencing datasets revealed
284 the MYC pathway as one of the most upregulated in MAIT cells. MYC is a critically
285 important transcription factor in conventional T cells, and acts as a metabolic master
286 regulator[23, 24, 26]. Experiments using high-dimensional quantitative mass spectrometry
287 on $CD4^+$ and $CD8^+$ T cells from wild type and MYC deficient mice reveal how MYC

288 controls TCR-driven cell growth and metabolism[23, 24]. We showed that MYC is a critical
289 regulator of human MAIT cell proliferation.
290
291 MAIT cell proliferation was triggered in a two-step process, where activation with 5-
292 ARU-MG, which forms the MAIT cell cognate antigen 5-OP-RU, did not drive MAIT cell
293 proliferation, but did trigger the expression of the high affinity IL-2 receptor, CD25.
294 Subsequent addition of IL-2 drove MAIT cell proliferation. A similar two-step process
295 occurs conventional $CD8^+$ T cells, in which IL-2 not required for the initiation of
296 proliferation but required for sustaining proliferation[43]. We also demonstrated that
297 increased expression of CD25 by activated MAIT cells was dependent on MYC, which
298 aligns with previous reports demonstrating that in MYC deficient conventional T cells,
299 the expression of CD25 does not increase upon stimulation[24].
300
301 MYC signalling is also essential for the upregulation of amino acid transporters on T
302 cells, including SLC7A5 [24]. We have previously reported that MAIT cells express
303 SLC7A5[27], and demonstrated here that inhibition of MYC results in diminished SLC7A5
304 and CD98 expression, and reduced transport of the SLC7A5 substrate kynurenine by
305 activated MAIT cells. Amino acid transport by SLC7A5/CD98 is critical for sustained
306 expression of MYC, suggesting a positive feed-forward loop[24]. Using the SLC7A5
307 inhibitor BCH we showed that amino acid transport through SLC7A5 is needed for
308 MAIT cell proliferation. This highlights the presence of a MYC-SLC7A5 axis present in
309 activated MAIT cells, similar to that identified in conventional T cells.
310
311 MYC also directs a glycolytic metabolism program in conventional T cells[23, 24, 26], that
312 is important for T cell growth, activation and effector functions[44]. Glycolytic
313 metabolism is required for MAIT cell cytokine and lytic molecule production [27, 37, 45],
314 but the factors regulating MAIT cell metabolism and the requirements for MAIT cell
315 proliferation are unknown. Herein we show that MAIT cells increase the expression of
316 key glycolytic enzymes (including HKII and LDH), supporting MAIT cell engagement of
317 glycolytic metabolism upon activation. Furthermore, inhibition of MYC resulted in
318 diminished HKII expression and rates of glycolytic metabolism, confirming that as in
319 conventional T cells, MYC is a key metabolic regulator. In conventional $CD8^+$ T cells,

320 glucose metabolism is also critical for cell growth and proliferation[46]. Herein we
321 demonstrated that glucose metabolism and glycolysis is needed for optimal MAIT cell
322 proliferation. Limiting glycolysis by acutely reducing glucose availability or substituting
323 glucose with galactose further provided evidence for glucose availability being a rate-
324 limiting step for proliferation in MAIT cells.
325
326 MAIT cell cytokine production is defective in numerous human diseases, including
327 cancer, obesity and COVID-19[8, 47, 48]. Here, we showed that MAIT cell proliferation was
328 reduced in people with obesity, which is consistent with reports of defective host
329 protection in obesity. Having demonstrated the importance of MYC and its targets for
330 MAIT cell proliferation, we investigated the impact of obesity on MYC, and observed
331 reduced MYC activity in MAIT cells from people with obesity. Furthermore, we
332 highlight that this is not due to reduced MYC mRNA expression in immune activated
333 MAIT cells from PWO. MYC protein has a short half-life due to constant proteasomal
334 degradation. Increased MYC protein levels are thus only seen in cells with sufficient
335 amino acid transport capable of fuelling protein synthesis in a self-fulfilling feed
336 forward loop[24, 25, 26, 49, 50]. We noted that expression of key MYC targets like SLC7A5
337 were also defective in MAIT cells isolated from people with obesity, as would be
338 expected with impaired MYC-driven transcription. We have previously demonstrated
339 that defects in glucose metabolism in both MAIT cells and NK cells from people with
340 obesity underlie blunted cytokine production of these cells [27, 28, 29]. The identification
341 of defective MYC expression in MAIT cells from people with obesity helps to further
342 understand these observations.
343
344 In conclusion, we have identified MYC as a regulator of MAIT cell metabolism. We
345 demonstrate that a MYC-SLC7A5-glycolysis axis is needed for MAIT cell proliferation
346 and that this is defective in obesity. However, this data extends beyond obesity and
347 provides insight into the molecular and metabolic regulation of MAIT cell proliferation
348 which will have particular relevance for the potential use of MAIT cells for
349 immunotherapy[21].
350

351 **Materials & methods**

352 **Study cohorts & ethical approval** A total cohort of 50 adults (25obese/25 non-obese)
353 were recruited. Inclusion criteria included ability to give informed consent, 18-65
354 years of age and a BMI<28 for the non-obese control cohort and BMI >30 for obese
355 cohort. Exclusion criteria for both cohorts included having a current or recent (<2
356 weeks) infection, being a current smoker, use of anti-inflammatory medications
357 including GLP-1 analogue therapies. Ethical approval was obtained from both St
358 Vincent's University Medical Ethics Committee and Maynooth University Ethics
359 Committee

360

361 **Preparation of peripheral blood mononuclear cells (PBMC) and flow cytometric**
362 **analysis** PBMC samples were isolated by density centrifugation over Ficoll from fresh
363 peripheral blood samples. MAIT cell staining was performed using specific surface
364 monoclonal antibodies (All Miltenyi Biotec) namely; CD3 (REA613), CD161 (REA631),
365 CD8 (REA734) and TCRVα7.2 (REA179) (Supplementary Figure 7) in addition to CD25
366 (REA570), CD71 (REA902) and CD98 (REA387). Cell populations were acquired using a
367 Attune NXT flow cytometer and analysed using FlowJo software (Treestar). Results are
368 expressed as a percentage of the parent population, as indicated and determined
369 using flow minus-1 (FMO) and unstained controls.

370

371 **MAIT cell proliferation analysis**. Fresh PBMC (1 x 10^6 /ml) were stimulated for 18
372 hours with 1 μg/mL of 5-ARU and 100 μM of Methylglyoxal, in the absence or presence
373 of specific metabolic inhibitors (2DG (2 mM), 10074-G5(10 μM), iBET762(10 μM) or
374 BCH(50 mM)). After 18 hours, RPMI 1640media was replaced with fresh culture media
375 containing IL-2 (33.3 ng/ml). Cultures were maintained for up to 28 days, replacing
376 media with fresh culture media containing IL-2 every 3 days. MAIT cell proliferation
377 was determined by either flow cytometric analysis of MAIT cell frequencies or cell
378 trace violet proliferation assays.

379

380 **MAIT cell proteomic sample preparation**. Purified IL-2 expanded MAIT cells ($MAIT^{IL-2}$)
381 were stimulated for 18 hours with anti-CD3/CD28 Dynabeads (Thermofisher), IL-12

382 (50 ng/ml) and IL-18 (50 ng/ml) for 18 hours. Cell pellets were lysed at room
383 temperature in 5% SDS, 50 mM TEAB pH8.5, 10mM TCEP under agitation for 30 mins,
384 then boiled for 5 mins and sonicated with a BioRuptor (30 seconds on, 30 seconds off
385 x 15 cycles). Protein concentration was determined using EZQ protein quantification
386 kit (Invitrogen) according to the manufacturer's protocol. Lysates were alkylated with
387 20 mM iodoacetamide for 1 hour at room temperature in the dark. The samples were
388 then processed using S-Trap micro columns (Protifi). 12% aqueous phosphoric acid
389 was added at 1:10 to each sample for a final concentration of ~1.2% phosphoric acid.
390 Samples were transferred to 5 ml lo-bind microcentrifuge tubes (Eppendorf). 3200µl
391 of S-Trap binding buffer (100 mM TEAB - pH 7.1 adjusted using phosphoric acid, 90%
392 MeOH) was added to each sample. Each sample was loaded onto an S-Trap column in
393 batches of 165 µl and centrifuged at 4,000 xg for 30 s or until all SDS lysate/S-Trap
394 buffer had passed through the S-Trap column. Loading and centrifuging of columns
395 was repeated until all the lysate was run through the column. Captured protein was
396 then washed by adding 150 µl S-trap binding buffer to columns, which were then spun
397 at 4,000 g for 30 s: columns were washed five times in total. Columns were transferred
398 to fresh 2ml collection tubes. 20 µl of digestion buffer (50mM ammonium bicarbonate
399 in HPLC water) containing 1:20 trypsin was added onto each column. Samples were
400 centrifuged at 4000g for 30 seconds and any solution that passed through was
401 returned to the top of the column. Tubes were incubated for 2 hrs at 47°C. 40 µL of
402 digestion buffer containing trypsin was added to each column. Samples were
403 centrifuged at 1,000 xg for 60 sec and the peptide elution kept. 40 µL of 0.2% aqueous
404 formic acid was added to the S-Trap protein-trapping matrix and centrifuged at 1,000
405 x g for 60 sec into the same collection tube. 40 µL of 50% aqueous acetonitrile
406 containing 0.2% formic acid was added and samples centrifuged at 4000 x g for 60
407 seconds for a final elution.

408 **Data independent acquisition (DIA) mass spectrometry acquisition.** An equivalent of
409 1.5 µg peptides were injected onto a nanoscale C18 reverse-phase chromatography
410 column coupled to an UltiMate 3000 RSLC nano, HPLC system (Thermo Fisher) and an
411 Orbitrap Exploris 480 Mass Spectrometer (Thermo Fisher). For liquid chromatography
412 the following buffers were used: buffer A (0.1% formic acid in Milli-Q water (v/v)) and

413 buffer B (80% acetonitrile and 0.1% formic acid in Milli-Q water (v/v). Samples were
414 loaded at 10 µL/min onto a trap column (100 µm × 2 cm, PepMap nanoViper C18
415 column, 5 µm, 100 Å, Thermo Scientific) equilibrated in 0.1% trifluoroacetic acid (TFA).
416 The trap column was washed for 3 min at the same flow rate with 0.1% TFA then
417 switched in-line with a Thermo Scientific, resolving C18 column (75 µm × 50 cm,
418 PepMap RSLC C18 column, 2 µm, 100 Å). Peptides were eluted from the column at a
419 constant flow rate of 300 nl/min with a linear gradient from 3% buffer B to 6% buffer
420 B in 5 min, then from 6% buffer B to 35% buffer B in 115 min, and finally to 80% buffer
421 B within 7 min. The column was then washed with 80% buffer B for 4 min and re-
422 equilibrated in 3% buffer B for 15 min. Two blanks were run between each sample to
423 reduce carry-over. The column was kept at a constant temperature of 50°C.

424 The data was acquired using an easy spray source operated in positive mode with
425 spray voltage at 2.6 kV, and the ion transfer tube temperature at 250°C. The MS was
426 operated in DIA mode. A scan cycle comprised a full MS scan (m/z range from 350-
427 1650), with RF lens at 40%, AGC target set to custom, normalised AGC target at 300%,
428 maximum injection time mode set to custom, maximum injection time at 20 ms,
429 microscan set to 1 and source fragmentation disabled. MS survey scan was followed
430 by MS/MS DIA scan events using the following parameters: multiplex ions set to false,
431 collision energy mode set to stepped, collision energy type set to normalized, HCD
432 collision energies set to 25.5, 27 and 30%, orbitrap resolution 30000, first mass 200,
433 RF lens 40%, AGC target set to custom, normalized AGC target 3000%, microscan set
434 to 1 and maximum injection time 55 ms. Data for both MS scan and MS/MS DIA scan
435 events were acquired in profile mode. The method used for the DIA mass
436 spectrometry was based on a previously published approach[51].
437

438 **DIA data quantification and analysis.** Quantification of reporter ions was completed
439 using Spectronaut (VX, Biognosys; Spectronaut 15.2.210819.50606) in library-free
440 (directDIA) mode. Minimum peptide length was set to 7 and maximum peptide length
441 was set to 52, with a maximum of 2 missed cleavages. MS1 and MS2 mass tolerance
442 strategy and XIC IM and RT extraction windows were set to dynamic, all with a
443 correction factor of 1. Trypsin was specified as the digestive enzyme used. The false

444 discovery rate at the precursor ion level and protein level was set at 1% (protein and
445 precursor Q-value cut-off). The max number of variable modifications was set to 5,
446 with protein N-terminal acetylation, and glutamine and asparagine deamidation set
447 as variable modifications. Carbamidomethylation of cysteine residues was selected as
448 a fixed modification. For calibration, the MS1 and MS2 mass tolerance strategy was
449 set to the system default. Machine learning was set to across experiment, with a
450 precursor PEP cut-off of 0.2, a protein Q-value cut-off of 0.01. Single-hit proteins were
451 not excluded, with single-hits defined by stripped sequence. For quantification, the
452 quantification method was set to QUANT 2.0. Inference correction was set to true with
453 MS1 min of 2 and MS2 min of 3. The major protein grouping was by protein group ID
454 and the minor peptide grouping was set to stripped sequence. Major and minor group
455 top N was set to false, with minor and major group quantities set to sum precursor
456 quantity and sum peptide quantity respectively. Quantity at the MS-level was set to
457 MS2 and quantity type to area. Proteotypicity filter was set to none, data filtering to
458 Q-value and cross run normalisation was switched off. MS2 demultiplexing was
459 automatic, the run limit for the directDIA library set to -1, with no profiling strategy or
460 unify peptide peaks strategy. Data filtering and protein copy number quantification
461 was performed in the Perseus software package, version 1.6.6.0. Copy numbers were
462 calculated using the proteomic ruler[30]. This method sets the summed peptide
463 intensities of the histones to the number of histones in a typical diploid cell. The ratio
464 between the histone peptide intensity and summed peptide intensities of all other
465 identified proteins is then used to estimate the protein copy number per cell for all
466 the identified proteins. Further filtration of the data was completed to include
467 proteins detected in at least ≥ 2 biological replicates, and exclude proteins identified
468 based on single peptides.
469
470 **Cell trace violet proliferation assay.** MAIT cell proliferation was also measured using
471 a CellTrace™ Violet (CTV) proliferation kit (ThermoFisher) according to the
472 manufacturer's instructions. Briefly, CellTrace solution was prepared immediately
473 prior to use to 5 mM stock using DMSO. Next the dye for diluted to 5 µM working
474 concentration by adding appropriate amount of the stock solution into pre-warmed
475 PBS. Isolated PBMC were stained at 10^6 cells per mL of the PBS-dye solution. Cells

476 were incubated for 20 min at room temperature, protected from light with circular
477 agitation. Unbound dye was washed away with RPMI1640, and cell were incubated
478 for at least 10 minutes to allow acetate hydrolysis of the dye. CTV stained cells were
479 stimulated for 18 hours with 1 μg/mL of 5-ARU and 100μM of methylglyoxal, in the
480 absence or presence of specific metabolic inhibitors (2DG (2mM), 10074-G5(10uM),
481 iBET762 (25 nM) or BCH (50 mM)). After 18 hours, media was replaced with fresh
482 culture media containing IL-2 (33.3 ng/ml). Cultures were maintained for 5 days before
483 analysis.
484
485 **MAIT cell metabolic analysis.** Fresh PBMC (1 x 10^6 /ml) or $MAIT^{IL-2}$ cells were activated
486 using Dynabeads, IL-12 (50 ng/ml) and IL-18 (50 ng/ml) for 18 hours. Cells were then
487 labelled for extracellular markers, then fixed and permeabilized using the True-
488 Nuclear Transcription Factor Buffer set (BioLegend) according to the manufacture's
489 instructions before intracellular staining with monoclonal antibodies specific for
490 hexokinase II (Abcam EPR20839), lactate dehydrogenase (Abcam EP1563Y) or MYC
491 (Cell Signalling D84C12).

492 **MAIT cell Seahorse experiments.** For real-time analysis of the extracellular
493 acidification rate (ECAR) of $MAIT^{IL-2}$ cells were cultured in the absence or presence of
494 stimulation (Dynabead, IL-12 & IL-18 (both 50 ng/ml) and the MYC inhibitor iBET762
495 (25 mM) for 18 hours before analysis on a Seahorse XF-96 Analyzer (Seahorse
496 Bioscience). In brief, 200,000 MAIT cells were adhered to a CellTaq (BD Pharmingen)
497 coated 96-well XF Cell Culture Microplate (Seahorse Biosciences). Sequential
498 measurements of ECAR following addition of the inhibitors (Sigma) oligomycin (2 μM)
499 and 2-deoxyglucose (2DG, 30 mM) allowed for the calculation of basal glycolysis. Each
500 cell culture condition was evaluated in quadruplicate, and 14 measurements were
501 made per sample.

502 **MAIT cell Kynurenine and BCH experiments.** MAIT cells activated for 18 hours
503 (Dynabeads and IL-12/IL-18 – both 50 ng/ml) in the absence or presence of a MYC
504 inhibitor (iBET 762 25 nM) were washed and resuspended in 200ml warmed HBSS
505 (1x10^6 cells) and incubated in a water bath at 37°C. Kynurenine (200 mM, in HBSS) was

506 warmed to 37°C, with a 4°C control and added as appropriate. Uptake was stopped
507 after 4 minutes by PFA (Final concentration 1%) for 30 mins at room temperature, in
508 the dark. After fixation, wash cells twice in PBS/0.5% BSA and resuspend in PBS/0.5%
509 BSA prior to acquisition on flow cytometer. The 405nm laser and 450/50 BP filter were
510 used for kynurenine fluorescence detection. For SLC7A5 inhibition experiments, the
511 concentration of amino acids in RPMI was diluted twofold using Hank's balanced salt
512 solution (HBSS; Invitrogen) in the presence or absence of BCH (50 mM; Sigma).

513 **PCR gene expression.** mRNA was extracted from MAIT cells from healthy controls and
514 PWO using EZNA Total RNA kit I (Omegabio-tek) according to the manufacturer's
515 protocol. Synthesis of cDNA was performed using qScript cDNA Synthesis kit
516 (QuantaBio). Real time RT-qPCR was performed using PerfeCTa SYBR Green FastMix
517 Reaction Mix (Green Fastmix, ROX^{TM}) (QuantaBio) and KiCqStart primer sets (Sigma).

518 **Western blotting analysis.** Human MAIT^{IL-2} cells ($2.5x10^6$) were cultured in 24-well
519 plates stimulated with various stimuli (Dynabeads, IL-2 (10-40 ng/ml) IL-12 (50 ng/ml)
520 and IL-18 (50 ng/ml) for 18 hours (in the absence or presence of STAT5 inhibitor (CAS
521 285986-31-4 Merck)) before harvesting for western blotting. Cells were lysed in NP-
522 40 lysis buffer (50mM Tris-HCl, pH 7.4, containing 150 mM NaCl, 1% (w/v) IGEPAL
523 (Sigma), and complete protease inhibitor mixture (Roche)). Samples were resolved
524 using SDS-PAGE and transferred to nitrocellulose membranes before analysis with
525 anti-MYC (Cell Signalling) anti-β-Actin (Sigma) antibodies. Protein bands were
526 visualised using enhanced chemiluminescence.
527

528 **In silico RNA sequencing analysis.** Publicly available RNA sequencing data sets of MAIT
529 cells were downloaded from Gene Expression Omnibus (GEO) accession number
530 GSE123805[11] (Hinks *et al.,* 2019) and National Center for Biotechnology Information
531 (NCBI) Sequence Read Archive (SRA) accession number PRJNA559574 [10]. Raw read
532 counts were downloaded from GEO[11] and the data analysis pipeline to this point is
533 detailed in the associated paper. Whereas raw sequencing data in format of FASTQ
534 files were downloaded from the NCBI SRA [10] and the following data analysis pipeline
535 was implemented. The TrimGalore (v0.6.6) tool was used with Cutadapt (v1.15) and

536 FastQC to apply quality and adapter trimming to FASTQ files. STAR (v2.7.9a) was used
537 to align trimmed reads to the human genome (*Homo sapiens* high coverage assembly
538 GRCh38 from the Genome Reference Consortium – GRCh38.p13) with the quantMode
539 GeneCounts option to output read counts per gene. The Bioconductor package EdgeR
540 (v3.28.1) was applied in R (v3.6.3) to identify statistically significant differentially
541 expressed genes between patient groups. Biological and technical variation was
542 accounted for by the negative binomial distribution of RNAseq count data using a
543 generalization of the Poisson distribution model. The filterByExpr function was applied
544 to remove lowly expressed genes. The data was normalized across library sizes,
545 between samples using the trimmed mean of M-values (TMM) normalization method.
546 Tagwise dispersions were estimated for the normalized dataset. *P*-values from
547 multiple comparisons were corrected with the Benjamini-Hochberg method in EdgeR.
548 For the comparisons between stimulations and controls, genes were considered
549 significantly differentially expressed with an FDR adjusted *p*-value < 0.1. Variance
550 Modeling at the Observational Level (VOOM) method within edgeR was used to
551 output normalized read counts as LogCPM values. These were used to perform
552 hierarchical clustering and to construct heatmaps in Gene Pattern's online server
553 (v3.9.11) and to perform Gene Set Enrichment Analysis (GSEA) (v4.1.0) with annotated
554 HALLMARK genesets from the MSigDB (Molecular Signatures Database) collections
555 (v6.2). Venn diagrams were constructed using InteractiVenn[52].
556
557 **Statistics.** Statistical analysis was completed using Graph Pad Prism 6 Software (USA).
558 Data is expressed as SEM. We determined differences between two groups using
559 student t-test and Mann Whitney U test where appropriate. Analysis across 3 or more
560 groups was performed using ANOVA. Correlations were determined using linear
561 regression models and expressed using Pearson or Spearman's rank correlation
562 coefficient, as appropriate. P values were expressed with significance set at <0.05.
563
564 **REFERENCES**
565
566 1. Godfrey, D.I., Koay, H.F., McCluskey, J. & Gherardin, N.A. The biology and
567 functional importance of MAIT cells. *Nat Immunol* **20**, 1110-1128 (2019).
568

2. Le Bourhis, L. *et al.* Antimicrobial activity of mucosal-associated invariant T cells. *Nat Immunol* **11**, 701-708 (2010).

3. van Wilgenburg, B. *et al.* MAIT cells are activated during human viral infections. *Nature communications* **7**, 11653 (2016).

4. Treiner, E. *et al.* Selection of evolutionarily conserved mucosal-associated invariant T cells by MR1. *Nature* **422**, 164-169 (2003).

5. Kjer-Nielsen, L. *et al.* MR1 presents microbial vitamin B metabolites to MAIT cells. *Nature* **491**, 717-723 (2012).

6. Provine, N.M. & Klenerman, P. MAIT Cells in Health and Disease. *Annu Rev Immunol* **38**, 203-228 (2020).

7. Gapin, L. Check MAIT. *J Immunol* **192**, 4475-4480 (2014).

8. O'Neill, C., Cassidy, F.C., O'Shea, D. & Hogan, A.E. Mucosal Associated Invariant T Cells in Cancer-Friend or Foe? *Cancers (Basel)* **13** (2021).

9. Leng, T. *et al.* TCR and Inflammatory Signals Tune Human MAIT Cells to Exert Specific Tissue Repair and Effector Functions. *Cell reports* **28**, 3077-3091.e3075 (2019).

10. Lamichhane, R. *et al.* TCR- or Cytokine-Activated CD8. *Cell reports* **28**, 3061-3076.e3065 (2019).

11. Hinks, T.S.C. *et al.* Activation and In Vivo Evolution of the MAIT Cell Transcriptome in Mice and Humans Reveals Tissue Repair Functionality. *Cell reports* **28**, 3249-3262 e3245 (2019).

12. Slichter, C.K. *et al.* Distinct activation thresholds of human conventional and innate-like memory T cells. *JCI insight* **1** (2016).

13. Chiba, A. *et al.* Mucosal-associated invariant T cells promote inflammation and exacerbate disease in murine models of arthritis. *Arthritis Rheum* **64**, 153-161 (2012).

14. Carolan, E. *et al.* Altered distribution and increased IL-17 production by mucosal-associated invariant T cells in adult and childhood obesity. *J Immunol* **194**, 5775-5780 (2015).

15. Cosgrove, C. *et al.* Early and nonreversible decrease of CD161++ /MAIT cells in HIV infection. *Blood* **121**, 951-961 (2013).

16. Leeansyah, E. *et al.* Activation, exhaustion, and persistent decline of the antimicrobial MR1-restricted MAIT-cell population in chronic HIV-1 infection. *Blood* **121**, 1124-1135 (2013).

17. Kang, S.J. *et al.* Activation, Impaired Tumor Necrosis Factor-alpha Production, and Deficiency of Circulating Mucosal-Associated Invariant T Cells in Patients with Scrub Typhus. *PLoS Negl Trop Dis* **10**, e0004832 (2016).

18. Bergin, R. *et al.* Mucosal-associated invariant T cells are associated with insulin resistance in childhood obesity, and disrupt insulin signalling via IL-17. *Diabetologia* (2022).

19. Gutierrez-Arcelus, M. *et al.* Lymphocyte innateness defined by transcriptional states reflects a balance between proliferation and effector functions. *Nature communications* **10**, 687 (2019).

20. Howson, L.J. *et al.* MAIT cell clonal expansion and TCR repertoire shaping in human volunteers challenged with Salmonella Paratyphi A. *Nature communications* **9**, 253 (2018).

21. Parrot, T. *et al.* Expansion of donor-unrestricted MAIT cells with enhanced cytolytic function suitable for TCR-redirection. *JCI insight* (2021).

22. Newsholme, E.A., Crabtree, B. & Ardawi, M.S. The role of high rates of glycolysis and glutamine utilization in rapidly dividing cells. *Biosci Rep* **5**, 393-400 (1985).

23. Wang, R. *et al.* The transcription factor Myc controls metabolic reprogramming upon T lymphocyte activation. *Immunity* **35**, 871-882 (2011).

24. Marchingo, J.M., Sinclair, L.V., Howden, A.J. & Cantrell, D.A. Quantitative analysis of how Myc controls T cell proteomes and metabolic pathways during T cell activation. *Elife* **9** (2020).

25. Sinclair, L.V. *et al.* Control of amino-acid transport by antigen receptors coordinates the metabolic reprogramming essential for T cell differentiation. *Nat Immunol* **14**, 500-508 (2013).

26. Preston, G.C. *et al.* Single cell tuning of Myc expression by antigen receptor signal strength and interleukin-2 in T lymphocytes. *The EMBO journal* **34**, 2008-2024 (2015).

27. O'Brien, A. *et al.* Obesity Reduces mTORC1 Activity in Mucosal-Associated Invariant T Cells, Driving Defective Metabolic and Functional Responses. *J Immunol* **202**, 3404-3411 (2019).

28. Tobin, L.M. *et al.* NK cells in childhood obesity are activated, metabolically stressed, and functionally deficient. *JCI insight* **2** (2017).

29. Michelet, X. *et al.* Metabolic reprogramming of natural killer cells in obesity limits antitumor responses. *Nat Immunol* **19**, 1330-1340 (2018).

30. Wisniewski, J.R., Hein, M.Y., Cox, J. & Mann, M. A "proteomic ruler" for protein copy number and concentration estimation without spike-in standards. *Mol Cell Proteomics* **13**, 3497-3506 (2014).

31. Howden, A.J.M. *et al.* Quantitative analysis of T cell proteomes and environmental sensors during T cell differentiation. *Nat Immunol* **20**, 1542-1554 (2019).

32. Hukelmann, J.L. *et al.* The cytotoxic T cell proteome and its shaping by the kinase mTOR. *Nat Immunol* **17**, 104-112 (2016).

33. Cornish, G.H., Sinclair, L.V. & Cantrell, D.A. Differential regulation of T-cell growth by IL-2 and IL-15. *Blood* **108**, 600-608 (2006).

34. Amati, B. *et al.* Oncogenic activity of the c-Myc protein requires dimerization with Max. *Cell* **72**, 233-245 (1993).

35. Yap, J.L. *et al.* Pharmacophore identification of c-Myc inhibitor 10074-G5. *Bioorg Med Chem Lett* **23**, 370-374 (2013).

36. Grimm, D. *et al.* Modulation of cellular energetics by galactose and pioglitazone. *Cell Tissue Res* **369**, 641-646 (2017).

37. Brien, A.O. *et al.* Targeting mitochondrial dysfunction in MAIT cells limits IL-17 production in obesity. *Cell Mol Immunol* (2020).

38. Magalhaes, I. *et al.* Mucosal-associated invariant T cell alterations in obese and type 2 diabetic patients. *J Clin Invest* **125**, 1752-1762 (2015).

39. Toubal, A., Nel, I., Lotersztajn, S. & Lehuen, A. Mucosal-associated invariant T cells and disease. *Nat Rev Immunol* (2019).

40. Godfrey, D.I., Le Nours, J., Andrews, D.M., Uldrich, A.P. & Rossjohn, J. Unconventional T Cell Targets for Cancer Immunotherapy. *Immunity* **48**, 453-473 (2018).

41. Schubert, K. *et al.* A Multi-Omics Analysis of Mucosal-Associated-Invariant T Cells Reveals Key Drivers of Distinct Modes of Activation. *Front Immunol* **12**, 616967 (2021).

42. Bulitta, B. *et al.* Proteomic definition of human mucosal-associated invariant T cells determines their unique molecular effector phenotype. *Eur J Immunol* **48**, 1336-1349 (2018).

43. D'Souza, W.N. & Lefrançois, L. IL-2 is not required for the initiation of CD8 T cell cycling but sustains expansion. *J Immunol* **171**, 5727-5735 (2003).

44. O'Neill, L.A., Kishton, R.J. & Rathmell, J. A guide to immunometabolism for immunologists. *Nat Rev Immunol* **16**, 553-565 (2016).

45. Zinser, M.E. *et al.* Human MAIT cells show metabolic quiescence with rapid glucose-dependent upregulation of granzyme B upon stimulation. *Immunol Cell Biol* (2018).

46. Sanchez, J., Jackson, I., Flaherty, K.R., Muliaditan, T. & Schurich, A. Divergent Impact of Glucose Availability on Human Virus-Specific and Generically Activated CD8 T Cells. *Metabolites* **10** (2020).

47. Magalhaes, I., Kiaf, B. & Lehuen, A. iNKT and MAIT Cell Alterations in Diabetes. *Front Immunol* **6**, 341 (2015).

48. McCarthy, C., O'Donnell, C.P., Kelly, N.E.W., O'Shea, D. & Hogan, A.E. COVID-19 severity and obesity: are MAIT cells a factor? *Lancet Respir Med* **9**, 445-447 (2021).

49. Swamy, M. *et al.* Glucose and glutamine fuel protein O-GlcNAcylation to control T cell self-renewal and malignancy. *Nat Immunol* **17**, 712-720 (2016).

50. Sinclair, L.V. *et al.* Antigen receptor control of methionine metabolism in T cells. *Elife* **8** (2019).

51. Muntel, J. *et al.* Surpassing 10 000 identified and quantified proteins in a single run by optimizing current LC-MS instrumentation and data analysis strategy. *Mol Omics* **15**, 348-360 (2019).

52. Heberle, H., Meirelles, G.V., da Silva, F.R., Telles, G.P. & Minghim, R. InteractiVenn: a web-based tool for the analysis of sets through Venn diagrams. *BMC Bioinformatics* **16**, 169 (2015).

Acknowledgements: The authors would like to thank all the donors and patients for supporting this project.

Funding Source: This study is supported by the National Children's Research Centre. NKM is supported by Health Research Board (ILP-POR-2019-110). CB is supported by a fellowship from Irish Research Council. Financial support for the Attune NxT was provided to Maynooth University Department of biology by Science Foundation Ireland (16/RI/3399). The proteomic research was supported by a Wellcome Trust Equipment Award to Prof Doreen A. Cantrell (202950/Z/16/Z).

Contributors Statement: NKM, MMP, CR, RB, NAW, CDB and CON performed the experiments and carried out analysis and approved the final manuscript as submitted. NV and GSB provided MAIT cell reagents and aided in the design of MAIT cell activation experiments. CF performed the in silico RNA sequencing analysis. NWK and DOS recruited patient cohorts and provided relevant clinical data. AEH, NJ, DOS & LVS

760 conceptualized and designed the study, analyzed the data, drafted the manuscript,
761 and approved the final manuscript as submitted.

762 **Competing Interest:** The authors declare no conflict of interest.

763 **Data Availability: All data needed to evaluate the conclusions in the paper are**
764 **present in the paper or the Supplementary Materials.** All data is available from the
765 corresponding author in line with ethical approval. Proteomic Data is deposited at
766 XXXX
767
768
769 **Figure Legends**
770
771 **Figure 1. Remodelling of MAIT cell proteome after activation.** (A) Proteins from IL-2
772 expanded MAIT ($MAIT^{IL-2}$) cells were ranked by mass contribution and the mean
773 cumulative protein mass was plotted against protein rank (n=4). (B) Table outlining
774 the total number of proteins detected in $MAIT^{IL-2}$ cells and their change upon
775 stimulation ($MAIT^{STIM}$; 18 hours with antiCD3/CD28 beads and 50ng/ml IL-12 & IL-18)
776 using quantitative proteomics (n=4 per group). (C) Protein mass in $MAIT^{IL-2}$ or
777 $MAIT^{STIM}$(n=4). (D) Scatter plot showing ex vivo MAIT cell size (Forward scatter) basally
778 or stimulated (as above)(n=15). (E) Heatmap of the proteome of $MAIT^{IL-2}$ and $MAIT^{STIM}$
779 cells (as above) (n=4/group). Relative protein abundance is graded from blue (low) to
780 red (high) per row. Key MAIT cell proteins (IL-18R1, KLRB1, DPPIV & TRAV1-2) are
781 represented in scatter graphs and their position in the heatmap is denoted by
782 arrows)(n=4/group). (F) Scatter plot displaying the copy numbers against fold change
783 of the $MAIT^{STIM}$ cell proteome compared with $MAIT^{IL-2}$ (Green circles represent
784 proteins increased more than 1.5 fold over $MAIT^{IL-2}$ cells). (G) Pie chart showing
785 proportional pathway analysis based on the $MAIT^{STIM}$ cell proteome (Analysis
786 performed with Panther – Raw data in supplementary file 1). * $p<0.05$, ** $p<0.01$ and
787 *** $p<0.001$.
788
789 **Figure 2. Activation of MYC and its target pathways in MAIT cells.** (A) GSEA plot
790 showing the increase in MYC targets gene expression in activated MAIT cells. Data
791 extrapolated from previously published RNA sequence dataset[10] on ex vivo MAIT cells
792 stimulated through TCR. (B) Heatmap displaying expression amounts of MYC-target
793 in basal ($MAIT^{IL-2}$) or stimulated ($MAIT^{STIM}$; 18hr antiCD3/CD28 beads + 50ng/ml IL-12
794 & IL-18) cells as determined by quantitative proteomics (n=4 per group). Relative
795 protein abundance is graded from grey (low) to green (high) per row. (C) Proteomic
796 determination of MYC protein expressed as copies per cell from basal ($MAIT^{IL-2}$) or
797 stimulated ($MAIT^{STIM}$) cells (n=4 per group) (Note identification based on single
798 peptide hit). (D-E) Western blot and densitometry displaying MYC expression in
799 $MAIT^{IL-2}$ or stimulated (as above) $MAIT^{STIM}$ cells (n=4). (F-G) Representative flow
800 cytometry histogram (F) (Mean Fluorescence Intensity (MFI) values are shown within
801 histogram) and MFI values (G) of MYC expression in $MAIT^{EX\ VIVO}$ cells (black) or
802 $MAIT^{STIM}$ (green) (n=4). (H) Heatmap displaying MYC target genes in $MAIT^{EX\ VIVO}$ cells
803 with or without TCR stimulation. Data extrapolated from previously published RNA

804 sequence dataset[11]. (I-K) Scatter plots showing STAT3, STAT5a, STAT5b protein levels
805 expressed as copies per cell from basal ($MAIT^{IL-2}$) or stimulated ($MAIT^{STIM}$) cells
806 (n=4/group). (L-M) Western blot and densitometry displaying MYC expression in
807 $MAIT^{IL-2}$ or $MAIT^{STIM}$ cells in the absence or presence of a STAT5i (n=3). * p<0.05, **
808 p<0.01 and *** p<0.001.
809
810 **Figure 3. IL-2 driven proliferation of MAIT cells is dependent on MYC.** (A) The
811 frequency of MAIT cells (as a percentage of total T cells) after stimulation of PBMC
812 ($1x10^6$) with antigenic stimulation (cognate antigen 5-ARUand Methylglyoxal) for 7
813 days (n=6). (B-C) Representative flow cytometry histogram and scatter plot showing
814 CD25 (IL-2RA) expression on $MAIT^{ex\ vivo}$ or stimulated through the TCR using
815 antiCD3/CD28 beads/IL-12 & IL18 ($MAIT^{STIM}$) for 18 hours (n=9). (D) CD25 protein
816 expressed as copies per cell from $MAIT^{IL-2}$ cells basally or $MAIT^{STIM}$ (n=4). (E) Graph
817 demonstrating frequency of MAIT cells (represented as percentage of T cells) after
818 stimulation with 5-ARU (1ug/ml) and Methylglyoxal (100μM) in the absence or
819 presence of IL-2 (33.3ng/ml) for 7 days (n=5). (F-G) Representative flow cytometry dot
820 plot and scatter plot showing MAIT cell frequencies after 7 days stimulation with 5-
821 ARU, Methylglyoxal and IL-2 (n=10). (H) MFI of CD25 expression on MAIT cells after 18
822 hours stimulation (as in C) in the absence or presence of the MYC inhibitor (10074-G5,
823 10uM) (n=5). (I) $MAIT^{IL-2}$ cell frequency after 7 days expansion (as in E) in the absence
824 of presence of the MYC inhibitor 10074-G5 (10uM) (n=8). (J) Forward scatter MFI of
825 MAIT cells after stimulation (as in C) in the absence of presence of the MYC inhibitor
826 10074-G5 (n=5). * p<0.05, ** p<0.01 and *** p<0.001.
827
828
829 **Figure 4. SLC7A5 facilitates MAIT cell proliferation and is dependent on MYC.** (A)
830 Mean protein copy number per cell of SLC7A5 in $MAIT^{IL-2}$ cells and in cells stimulated
831 for 18hrs ($MAIT^{STIM}$; antiCD3/CD28 beads/IL-12 & IL18) (n=4). (B) Scatter plot showing
832 SLC7A5 mRNA expression in $MAIT^{IL-2}$ cells or $MAIT^{STIM}$ (as in A) (n=12). (C) Flow
833 cytometry MFI data of CD98 expression on ex vivo MAIT cells or stimulated for 18 hrs
834 (as in A)(n=7). (D) Mean protein copy number per cell of SLC3A52 in basal or
835 stimulated $MAIT^{IL-2}$ cells (n=4/group). (E) Flow cytometry data of uptake of kynurenine
836 into ex vivo MAIT cells (n=5). (F) SLC7A5 mRNA expression in $MAIT^{IL-2}$ cells and
837 $MAIT^{STIM}$ (as in A) in the absence or presence of the MYC specific inhibitor 10074-G5
838 (n=5). (G) Flow cytometry MFI expression of CD98 on ex vivo MAIT cells after
839 stimulation (as in A) in the absence or presence of the MYC specific inhibitor 10074-
840 G5 (10uM) (n=5). (H) Flow cytometry data of uptake of kynurenine into $MAIT^{IL-2}$ cells
841 stimulated for 18 hours (antiCD3/CD28 beads/IL-12 & IL18) in the absence or presence
842 of the MYC inhibitor iBET 762 (n=4). (I) The frequency of MAIT cells after 7 days
843 expansion with 5-ARU (1ug/ml) and Methylglyoxal (100μM) in the absence or
844 presence of IL-2 (33.ng/ml)) in the absence of presence of the SLC7A5 inhibitor BCH
845 (n=5). (J-K) Representative flow cytometry histogram and scatter plot showing cell
846 trace violet (CTV) MFI in MAIT cells after 5 days stimulation (as in G) in the absence of
847 presence of BCH (n=7). * p<0.05, ** p<0.01 and *** p<0.001.
848
849 **Figure 5. Glucose metabolism facilitates MAIT cell proliferation and is dependent on**
850 **MYC.** (A) Mean protein copy number per cell of Hexokinase-II (HKII) in $MAIT^{IL-2}$ and in

851 MAIT$^{IL2+STIM}$ (stimulated for 18 hours with antiCD3/CD28 beads and IL-18 (50ng/ml)
852 (n=4). (B-C) Representative flow cytometry histogram and MFI data of HKII in MAIT $^{ex-}$
853 ^{vivo} cells basally or stimulated (18 hours with antiCD3/CD28 beads and IL-18 (50ng/ml);
854 MAIT^{STIM})(n=8). (D) Flow cytometry MFI data of LDHA expression in MAIT $^{ex-vivo}$ and
855 MAIT^{STIM} cells (as in C) (n=8). (E) HKII mRNA expression in MAIT^{IL-2} and in MAIT$^{IL2+STIM}$
856 cells (as in A) in the absence of presence of the MYC specific inhibitor 10074-G5 (n=5).
857 (F-G) Representative Seahorse Analyzer trace and scatter plot detailing the ECAR rates
858 of MAIT^{IL-2} cells stimulated for 18 hours (antiCD3/CD28 beads/IL-12 & IL18) in the
859 absence or presence of the MYC inhibitor iBET 762 (n=4). (H) The frequency of MAIT
860 cells after 7 days expansion from PBMC (1x10^{6}) using cognate antigen 5-ARU (1ug/ml),
861 Methylglyoxal (100μM) and IL-2 (33.3ng/ml) in the absence of presence of the
862 glycolysis inhibitor 2DG (2mM) (n=5). (I-J) Representative flow cytometry histogram
863 and scatter plot showing cell trace violet (CTV) MFI in MAIT cells after 5 days
864 stimulation in the absence of presence of 2DG (n=5). (K-L) Representative flow
865 cytometry dot plot and MAIT cell frequencies after 7 days stimulation in media
866 containing either 10mM or 1mM glucose (n=3). (M) MAIT cell frequencies after 7 days
867 stimulation in media containing either 10mM glucose or 10mM galactose (n=6). *
868 p<0.05, ** p<0.01 and *** p<0.001.
869
870
871 **Figure 6. MYC is defective in obesity resulting in diminished MAIT cell proliferation.**
872 (A) The frequency of MAIT cells after 0-28 days expansion after 18 hour stimulation
873 with 5-ARU (1ug/ml), Methylglyoxal (100μM) and maintenance in IL-2 (33.3ng/ml) in
874 either healthy controls (green circles) or people with obesity (PWO) (grey circles)
875 (n=10/group). (B) Fold expansion of MAIT cells from healthy controls or people with
876 obesity after 7 days stimulation (with 5-ARU (1ug/ml), Methylglyoxal (100μM) and IL-
877 2 (33.3ng/ml)) (n=8). (C-D) Representative flow cytometry histogram (C) and MFI data
878 (D) of MYC expression in ex vivo MAIT cells from healthy controls (top panel,C) or PWO
879 (bottom panel,C) stimulated with antiCD3/CD28 beads and IL-18 (50ng/ml) for 18
880 hours (n=6-7/group). (E) Scatter graph showing MYC gene counts (extrapolated from
881 published RNA sequencing dataset[27]) in ex-vivo MAIT cells from health controls or
882 PWO (n=4-5/group). (F) Heatmap displaying MYC target genes in ex-vivo MAIT cells
883 from health controls or PWO (n=4-5/group). (G) CD25 expression (MFI) on ex-vivo
884 MAIT cells or stimulated MAIT cells (as in C) from either healthy controls or PWO (n=5-
885 8/group). (H) mRNA expression of *Slc7a5* in MAIT^{IL-2} cells or MAIT^{IL-2} stimulated (as in
886 C) from either healthy controls or PWO (n=6-10/group). (I) Scatter plot showing CD98
887 expression (MFI) on ex-vivo MAIT cells basally or stimulated (as in C) from either
888 healthy controls or PWO (n=3-4/group). (J) Scatter plot showing Kynurenine uptake
889 into MAIT cells from either healthy controls or PWO (n=5/group). * p<0.05, ** p<0.01
890 and *** p<0.001.
891
892 **Figure 7. Working Model.** Schematic outlining the proposed working model. Top
893 panel details a MYC-SLC7A5-Glycolysis axis in activated MAIT cells. Bottom panel
894 outlines the impact of obesity on the proposed MYC-SLC7A5-Glycolysis axis in
895 activated MAIT cells.
896

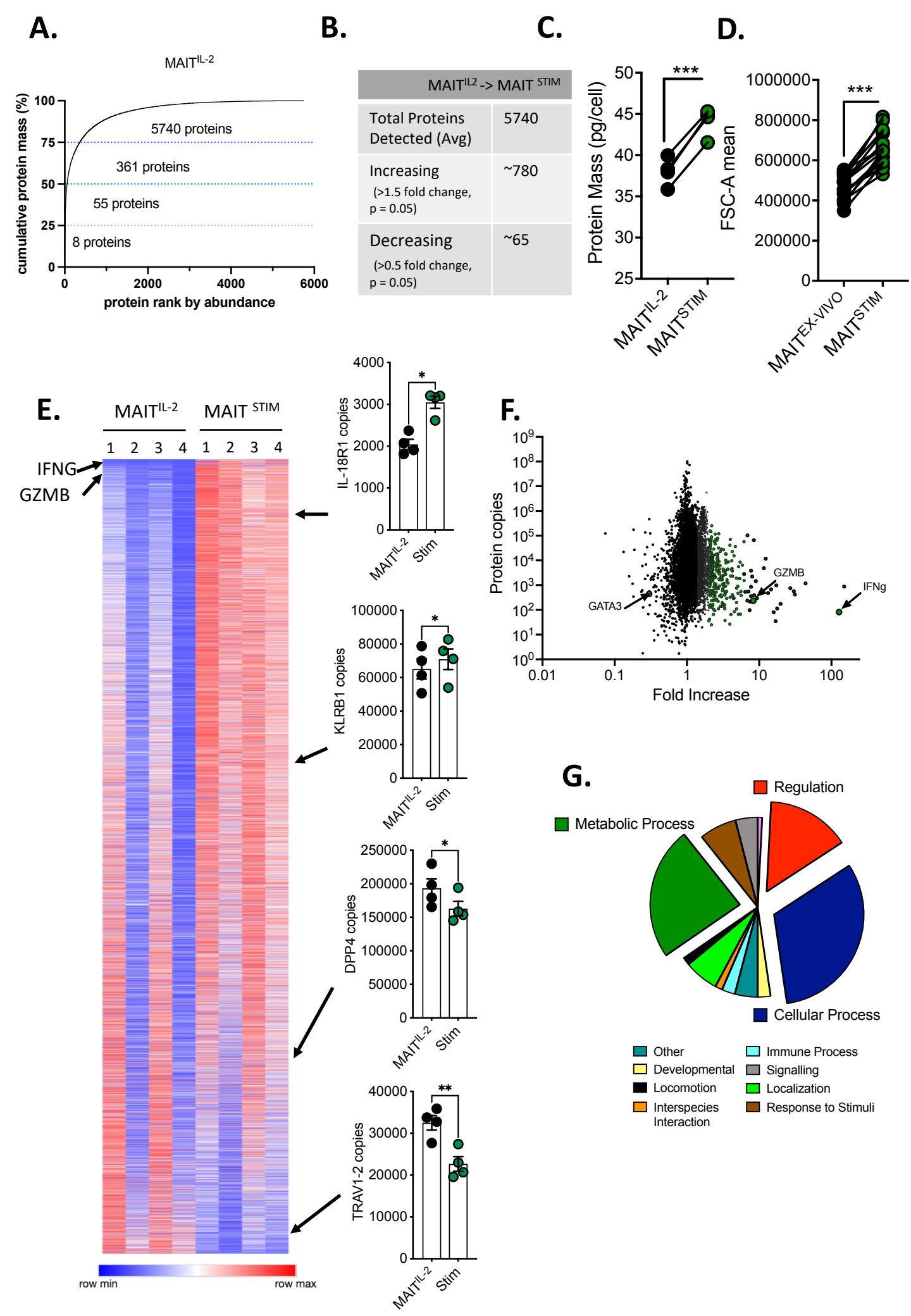

MAIT^IL2 -> MAIT STIM	
Total Proteins Detected (Avg)	5740
Increasing (>1.5 fold change, p = 0.05)	~780
Decreasing (>0.5 fold change, p = 0.05)	~65

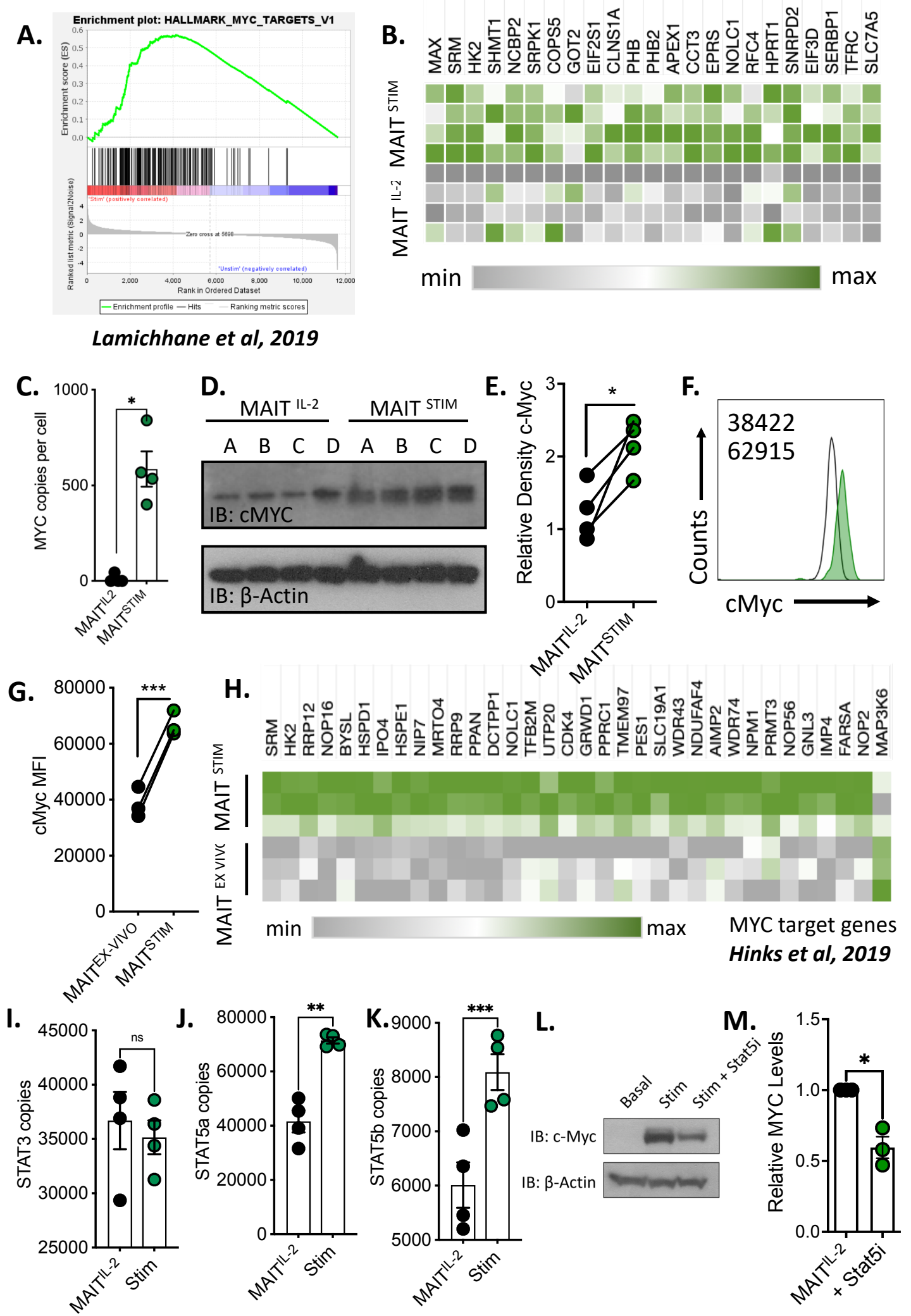
A.
Enrichment plot: HALLMARK_MYC_TARGETS_V1
Enrichment score (ES)
'Stim' (positively correlated)
Zero cross at 5698
'Unstim' (negatively correlated)
Ranked list metric (Signal2Noise)
Rank in Ordered Dataset
Enrichment profile
Hits
Ranking metric scores
B.
MAX
SRM
HK2
SHMT1
NCBP2
SRPK1
COPS5
GOT2
EIF2S1
CLNS1A
PHB
PHB2
APEX1
CCT3
EPRS
NOLC1
RFC4
HPRT1
SNRPD2
EIF3D
SERBP1
TFRC
SLC7A5
MAIT STIM
MAIT IL-2
min
max
Lamichhane et al, 2019
C.
MYC copies per cell
MAIT IL2
MAIT STIM
D.
MAIT IL-2
MAIT STIM
A B C D A B C D
IB: cMYC
IB: β-Actin
E.
Relative Density c-Myc
MAIT IL-2
MAIT STIM
F.
38422
62915
Counts
cMyc
G.
cMyc MFI
MAIT EX-VIVO
MAIT STIM
H.
SRM
HK2
RRP12
NOP16
BYSL
HSPD1
IPO4
HSPE1
NIP7
MRTO4
RRP9
PPAN
DCTPP1
NOLC1
TFB2M
UTP20
CDK4
GRWD1
PPRC1
TMEM97
PES1
SLC19A1
WDR43
NDUFAF4
AIMP2
WDR74
NPM1
PRMT3
NOP56
GNL3
IMP4
FARSA
NOP2
MAP3K6
MAIT STIM
MAIT EX VIVO
min
max
MYC target genes
Hinks et al, 2019
I.
STAT3 copies
ns
MAIT IL-2
Stim
J.
STAT5a copies
MAIT IL-2
Stim
K.
STAT5b copies
MAIT IL-2
Stim
L.
Basal
Stim
Stim + Stat5i
IB: c-Myc
IB: β-Actin
M.
Relative MYC Levels
MAIT IL-2
+ Stat5i

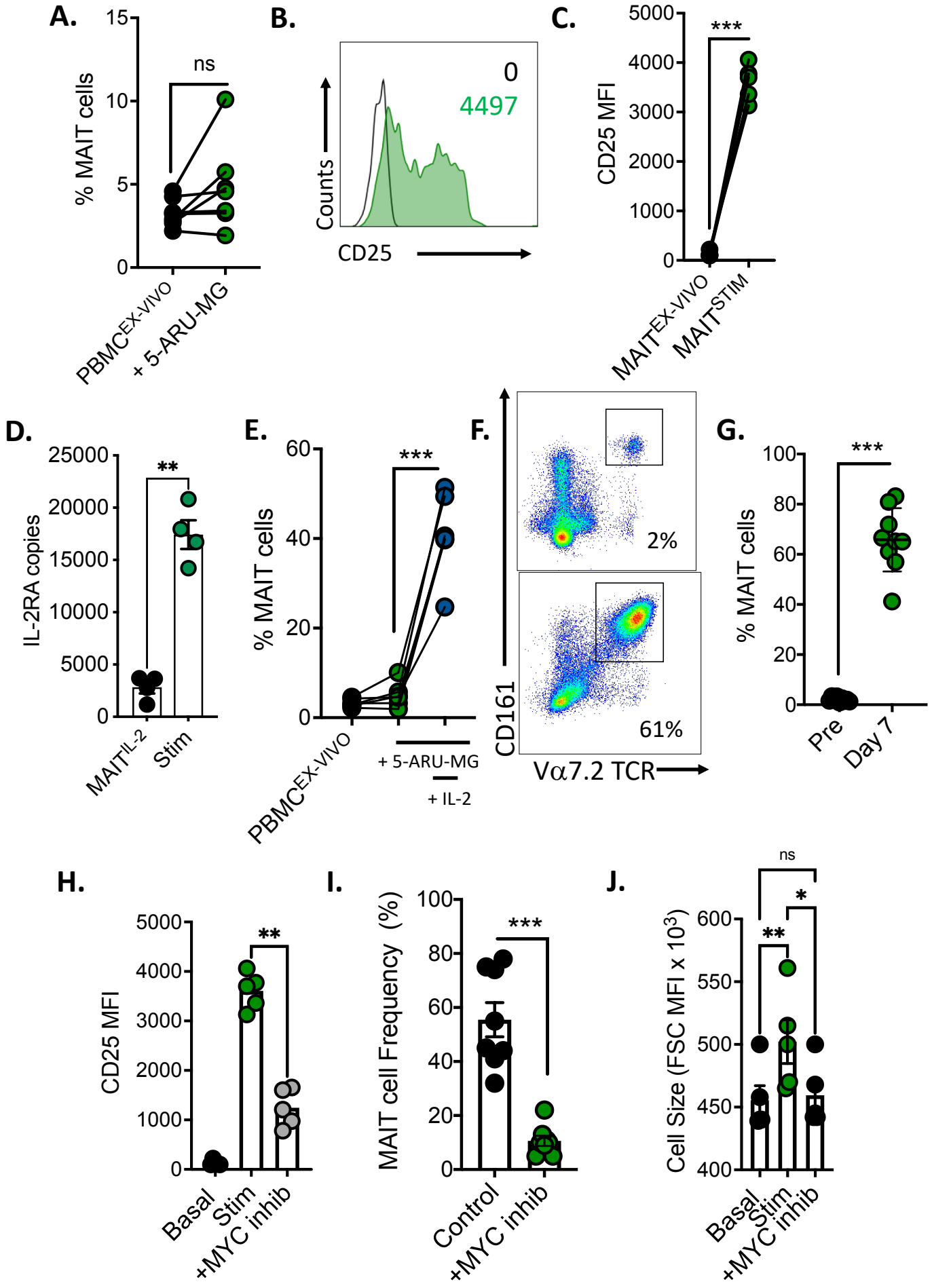
A.
% MAIT cells
ns
PBMC EX-VIVO
+ 5-ARU-MG
B.
Counts
CD25
0
4497
C.
CD25 MFI
***
MAIT EX-VIVO
MAIT STIM
D.
IL-2RA copies
**
MAIT IL-2
Stim
E.
% MAIT cells
***
PBMC EX-VIVO
+ 5-ARU-MG
+ IL-2
F.
CD161
Vα7.2 TCR
2%
61%
G.
% MAIT cells
***
Pre
Day 7
H.
CD25 MFI
**
Basal
Stim
+MYC inhib
I.
MAIT cell Frequency (%)
***
Control
+MYC inhib
J.
Cell Size (FSC MFI x 10³)
ns
**
*
Basal
Stim
+MYC inhib

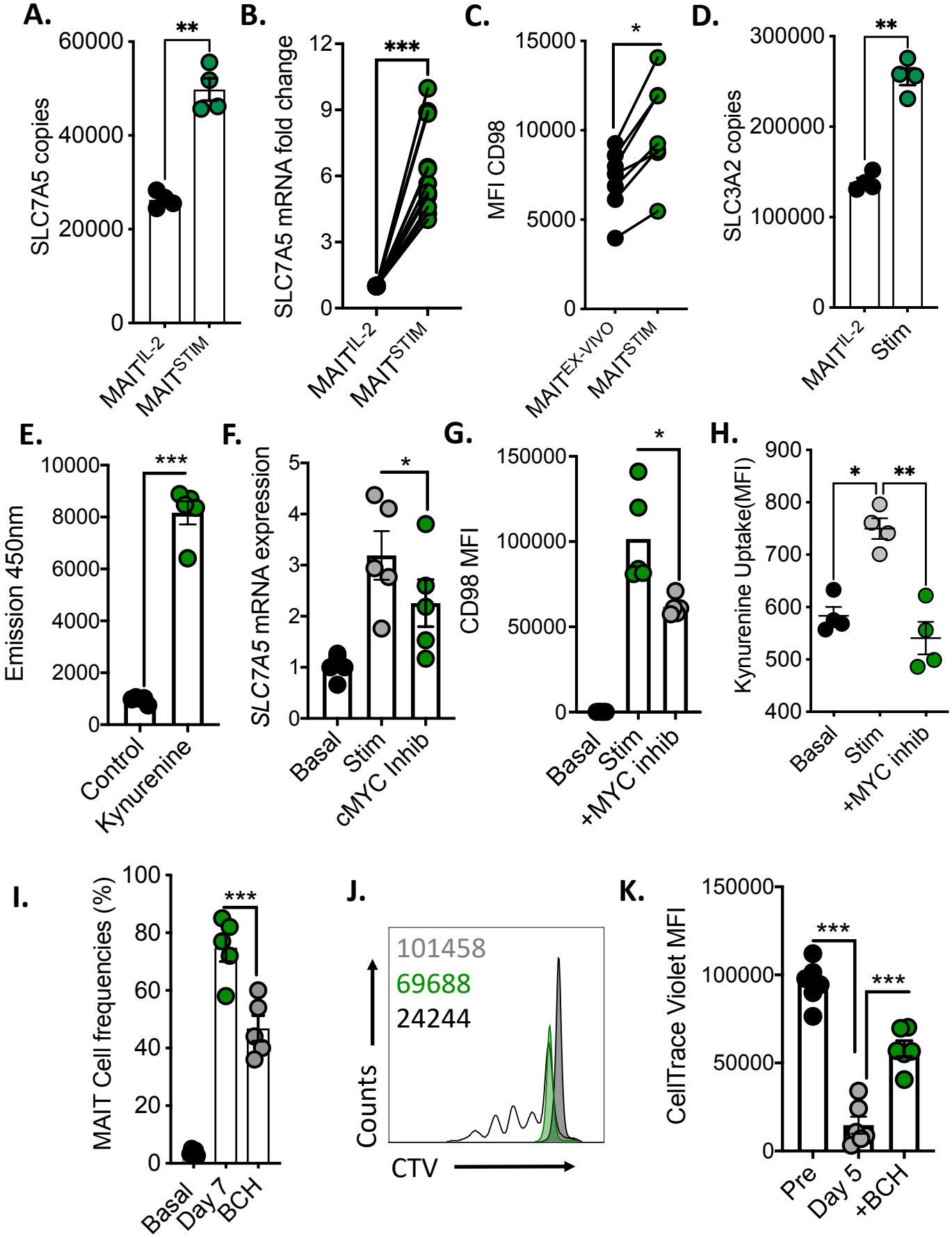
A.
SLC7A5 copies
60000
40000
20000
0
**
MAIT IL-2
MAIT STIM
B.
SLC7A5 mRNA fold change
12
9
6
3
0
***
MAIT IL-2
MAIT STIM
C.
MFI CD98
15000
10000
5000
0
*
MAIT EX-VIVO
MAIT STIM
D.
SLC3A2 copies
300000
200000
100000
0
**
MAIT IL-2
Stim
E.
Emission 450nm
10000
8000
6000
4000
2000
0
***
Control
Kynurenine
F.
SLC7A5 mRNA expression
5
4
3
2
1
0
*
Basal
Stim
cMYC Inhib
G.
CD98 MFI
150000
100000
50000
0
*
Basal
Stim
+MYC inhib
H.
Kynurenine Uptake(MFI)
900
800
700
600
500
400
*
**
Basal
Stim
+MYC inhib
I.
MAIT Cell frequencies (%)
100
80
60
40
20
0
***
Basal
Day 7
BCH
J.
101458
69688
24244
Counts
CTV
K.
CellTrace Violet MFI
150000
100000
50000
0
***
***
Pre
Day 5
+BCH

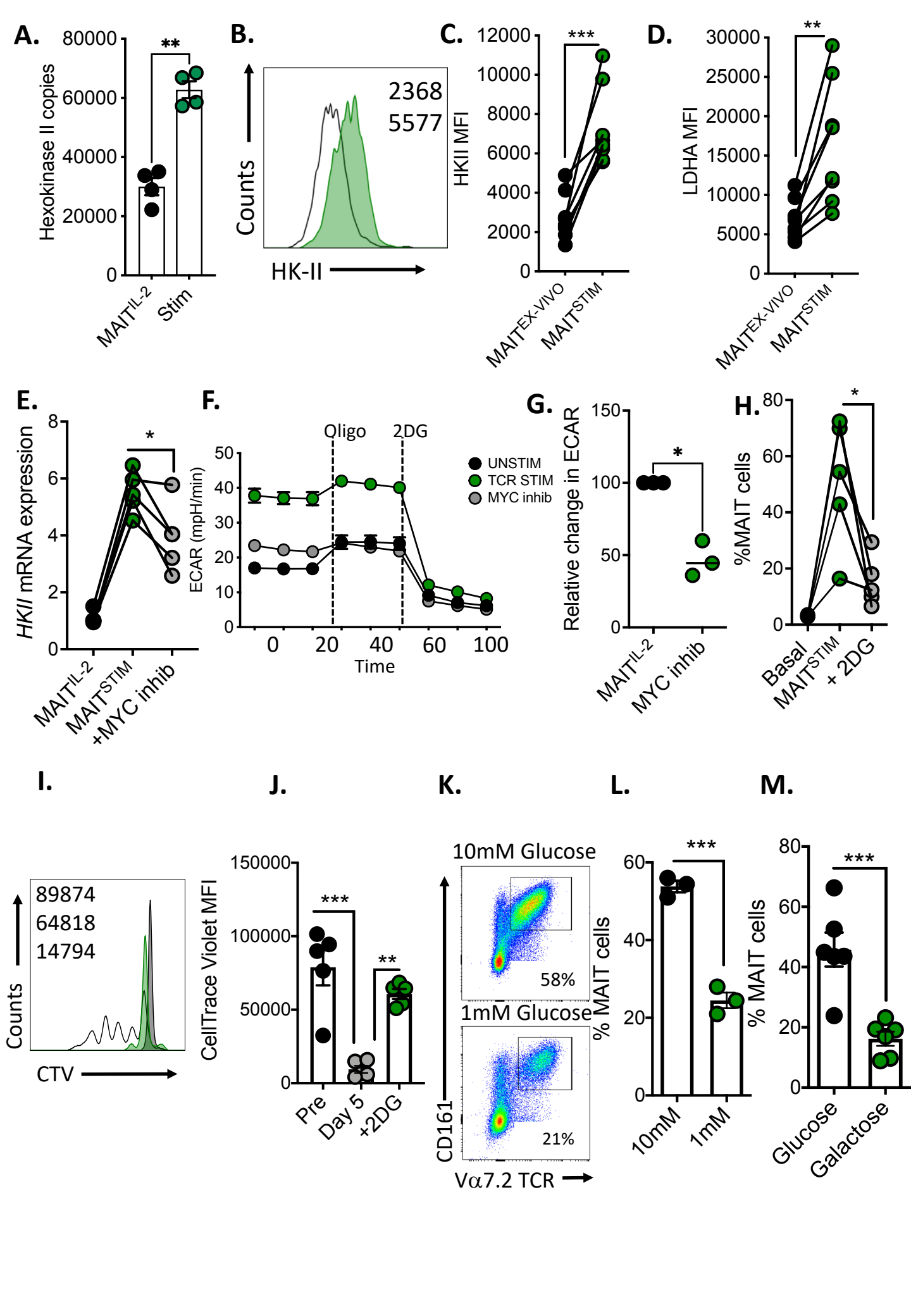
A.
Hexokinase II copies
80000
60000
40000
20000
0
**
MAIT^IL-2
Stim
B.
Counts
2368
5577
HK-II
C.
HKII MFI
12000
10000
8000
6000
4000
2000
0
***
MAIT^EX-VIVO
MAIT^STIM
D.
LDHA MFI
30000
25000
20000
15000
10000
5000
0
**
MAIT^EX-VIVO
MAIT^STIM
E.
HKII mRNA expression
8
6
4
2
0
*
MAIT^IL-2
MAIT^STIM
+MYC inhib
F.
ECAR (mpH/min)
50
40
30
20
10
0
Oligo
2DG
UNSTIM
TCR STIM
MYC inhib
0
20
40
60
100
Time
G.
Relative change in ECAR
150
100
50
0
*
MAIT^IL-2
MYC inhib
H.
%MAIT cells
80
60
40
20
0
*
Basal
MAIT^STIM
+ 2DG
I.
Counts
89874
64818
14794
CTV
J.
CellTrace Violet MFI
150000
100000
50000
0
***
**
Pre
Day 5
+2DG
K.
10mM Glucose
58%
1mM Glucose
21%
CD161
Vα7.2 TCR
L.
% MAIT cells
60
40
20
0
***
10mM
1mM
M.
% MAIT cells
80
60
40
20
0
***
Glucose
Galactose

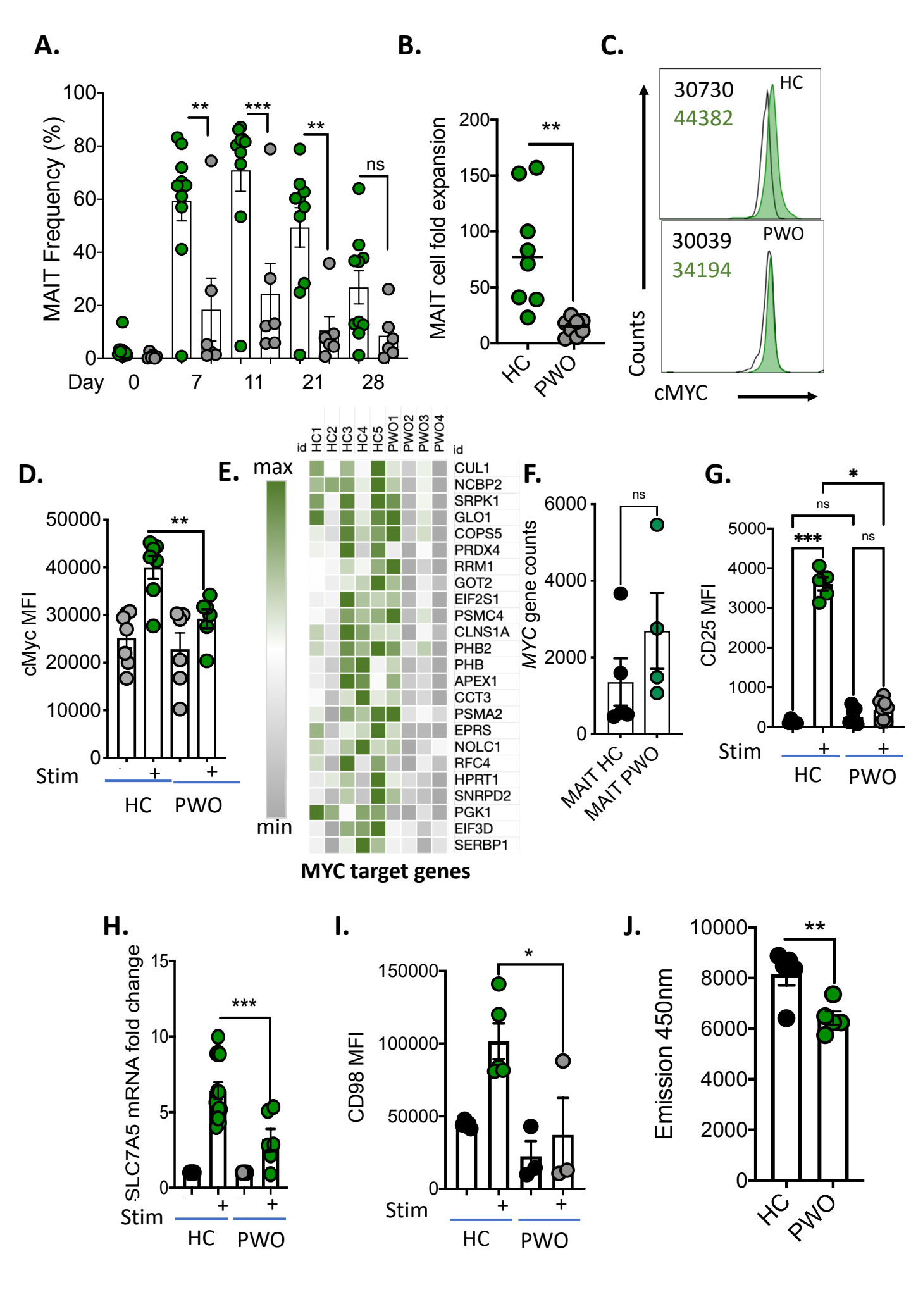
A.
MAIT Frequency (%)
Day
0
7
11
21
28
**
***
**
ns
B.
MAIT cell fold expansion
HC
PWO
**
C.
30730
44382
HC
30039
34194
PWO
Counts
cMYC
D.
cMyc MFI
Stim
HC
PWO
**
E.
max
min
id
HC1
HC2
HC3
HC4
HC5
PWO1
PWO2
PWO3
PWO4
CUL1
NCBP2
SRPK1
GLO1
COPS5
PRDX4
RRM1
GOT2
EIF2S1
PSMC4
CLNS1A
PHB2
PHB
APEX1
CCT3
PSMA2
EPRS
NOLC1
RFC4
HPRT1
SNRPD2
PGK1
EIF3D
SERBP1
MYC target genes
F.
MYC gene counts
MAIT HC
MAIT PWO
ns
G.
CD25 MFI
Stim
HC
PWO
***
ns
ns
*
H.
SLC7A5 mRNA fold change
Stim
HC
PWO
***
I.
CD98 MFI
Stim
HC
PWO
*
J.
Emission 450nm
HC
PWO
**